IJRCS

International Journal of Robotics and Control Systems
Vol. 5, No. 4, 2025, pp. 2085-2103
ISSN 2775-2658
http://pubs2.ascee.org/index.php/ijrcs

ASCEE

Bio-Inspired Optimization for Frequency Stability in Microgrids with Electric Vehicle Support: Towards Sustainability of Renewable Energy Systems

Mohamed F. Elnaggar [a,1,*]

[a] Department of Electrical Engineering, College of Engineering, Prince Sattam Bin Abdulaziz University, Al-Kharj 11942, Saudi Arabia
[1] mfelnaggar@yahoo.com
* Corresponding Author

ARTICLE INFO

Article history
Received May 27, 2025
Revised August 05, 2025
Accepted October 22, 2025

Keywords
Sustainable Development;
Microgrids;
Electric Vehicle;
Renewable Energy Sources;
Wave Search with the Balloon Effect Algorithm

ABSTRACT

The increasing integration of renewable energy sources (RES) such as solar and wind into modern microgrid systems has posed significant challenges for maintaining frequency stability, primarily due to their inherent variability and unpredictability. Conventional load frequency control (LFC) strategies, which depend on fixed system inertia and static tuning, often fail to cope with these highly dynamic conditions. In response, this study introduces an innovative hybrid control strategy that merges the Wave Search Algorithm (WSA) with the Balloon Effect (BE) model. This synergy is designed to support adaptive LFC in a multi-source microgrid comprising diesel generators, solar PV, and bi-directional electric vehicles (EVs). The WSA facilitates a balanced global and local search behavior, while the BE component enables structural adjustments in real-time by leveraging transfer function variations within the system. This integrated approach adaptively calibrates an integral controller to suppress frequency deviations and enhance overall system robustness. Through simulation of three realistic disturbance scenarios—namely, a sudden increase in load, an abrupt reduction in PV output, and a fluctuating load profile with EV contribution—the WSA+BE controller demonstrated clear superiority over classical techniques and alternative optimizers, including Jaya, SCO, GTO, and standalone WSA. Results show enhanced damping characteristics, quicker stabilization, and improved adaptability across all cases, confirming the proposed method's potential for reliable frequency control in RES-dominated microgrids.

1. Introduction

The accelerated increase in global energy demand since the industrial revolution has brought severe environmental consequences, prompting many nations to adopt ambitious net-zero emission policies [1]-[5]. As fossil fuel dependence declines, this transition is fundamentally reshaping energy infrastructure through the growing integration of renewable energy sources (RES) such as solar photovoltaic (PV) and wind power [6]-[8]. These clean, decentralized sources are increasingly deployed within multi-energy microgrids (μGs), which allow for flexible, localized energy management [9], [10]. By facilitating rapid deployment of distributed generation technologies, µGs offer operational independence, resiliency, and user-side engagement [11], [12]. Building on this context, the transition to RES introduces significant challenges to traditional power system control mechanisms, particularly in frequency regulation tasks [13]-[16].

While the environmental advantages of RES are indisputable, their dependence on fluctuating weather patterns introduces operational uncertainty. This is especially critical in islanded or semi-autonomous µGs, where the absence of large-scale centralized inertia severely limits the system's ability to self-stabilize under load and generation variations. In such configurations, the frequency deviation becomes more volatile due to the combined effect of variable generation and dynamic load behavior. Consequently, conventional frequency control strategies (originally designed for inertia-rich systems) fail to deliver adequate performance. These challenges motivate a deeper look into modern control paradigms and algorithmic advancements [17]-[26]. Several advanced techniques have emerged to tackle frequency stability in µGs. Traditional load frequency control (LFC) techniques rely on synchronous generator inertia, which diminishes as RES penetration increases [27]-[29]. To compensate for the inertia deficit, researchers have explored virtual inertia control (VIC), droop control, fuzzy logic, neural networks, and a variety of optimization-based adaptive controllers [30]-[35]. Notably, intelligent tuning of PID-type controllers using algorithms such as Jaya, Grey Wolf Optimizer (GWO), and recently, the Wave Search Algorithm (WSA) has gained traction, with objective functions formulated around performance indicators such as rise time, settling time, and overshoot [36]-[39]. However, despite these developments. Several unresolved limitations persist (particularly in adaptability and robustness).

Most of the current optimization strategies for LFC assume relatively stable operating conditions and are not well-suited for fast-changing environments typical of modern µGs. These methods often rely on precise system modeling, which may not hold under dynamic uncertainty or structural changes. Additionally, they tend to suffer from premature convergence or sensitivity to initial parameter settings, particularly in non-convex or multi-modal search spaces. There remains a need for real-time, structure-aware, and dynamically adaptive optimization techniques that can respond effectively to abrupt system disturbances. To clearly illustrate these shortcomings, Table 1 compares several studies, including recent optimization methods such as WSA, based on their adaptability, modeling reliance, and robustness under uncertainty.

Table 1. Comparison of LFC methods based on adaptability, robustness, and modeling reliance

Study / Method	Control Approach	Adaptive to Load/Gain Variations	Robust to Uncertainty	Modeling Dependence	Main Limitation
Jaya algorithm [40]	Static optimization	Low	Moderate	High	Premature convergence in complex conditions
GWO [41]	Population-based tuning	Moderate	Low	Moderate	Sensitive to initial settings
Fuzzy + ANN [42]	Soft computing hybrid	Moderate	Moderate	High	Complex implementation
VIC + Droop [25]	Virtual inertia	Low	Low	Low	Ineffective for large disturbances
Proposed WSA+BE (this work)	Hybrid dynamic optimization	High	High	Low	-

To address the aforementioned challenges, this study proposes a hybrid optimization framework that combines the WSA with the balloon effect (BE) mechanism. The WSA is inspired by wave propagation dynamics and is known for its strong global exploration and local exploitation balance, making it suitable for handling complex, multi-modal objective functions. On the other hand, the BE introduces structural interaction between the optimization objective and the dynamic behavior of the system, enabling the algorithm to respond adaptively to real-time disturbances. The proposed WSA+BE framework is used to tune an adaptive integral controller for frequency regulation in a multi-energy µG composed of DsG, solar PV units, and controllable loads. The hybrid approach leverages real-time system feedback and dynamic tuning to overcome the shortcomings of static and model-dependent optimization methods. Through comprehensive simulation studies, the performance of the proposed controller is compared against classical integral, Jaya-optimized, and standalone WSA-based controllers. The results demonstrate that the hybrid WSA+BE approach significantly enhances frequency stability, reduces deviation amplitudes, and improves adaptability under dynamic load and generation scenarios.

The key contributions of this research include: Development of a WSA+BE-based adaptive LFC mechanism. Integration of real-time feedback from the µG's open-loop transfer dynamics into the control strategy. Comparative validation with traditional and modern controllers under diverse operating profiles, highlighting improvements in robustness and real-time adaptability.

2. System Architecture, Dynamic Modeling, and Control Strategy Implementation

To analyze the frequency (F) dynamics of the proposed system, a detailed modeling framework of the µG is developed based on the block-level interconnection of all generation units. The frequency regulation mechanism, particularly for the PV component, is addressed through a sequential adaptation of the integral (I) controller, enhanced by the hybrid WSA+BE algorithm. The frequency error signal serves as the objective function (OF) in the optimization process, aiming to minimize fluctuations through a time-domain performance criterion, specifically the Integral of Squared Time multiplied by Squared Error (ISTSE-OF). To improve frequency stability, appropriate auxiliary sources are integrated into the µG, and the proposed control scheme is fine-tuned to mitigate the impact of external disturbances such as sudden load variations. This ensures sustained µG operation with minimal deviation from nominal frequency values [43]-[47].

2.1. LFC in µGs

Maintaining power balance between generation, load demand, and losses is essential for stable µG operation. Due to the dynamic nature of system operation, both power allocation and frequency can experience periodic deviations, potentially impacting system reliability. LFC is thus a critical aspect of µG design and implementation, working in tandem with automatic generation control. The main objectives of LFC include: eliminating steady-state frequency deviations during islanded operation, minimizing frequency fluctuations during transitions between grid-connected and islanded modes, enabling accurate disturbance detection, and optimizing dynamic response by reducing settling time and limiting overshoot/undershoot [48]-[51].

Given the nonlinear and time-varying characteristics of µGs, a linearized model is typically used to analyze frequency responses to small load disturbances. These responses typically span time scales ranging from a few seconds to several minutes, making them significantly slower than variations in rotor angle and terminal voltage. Accordingly, simplified models (most commonly first-order transfer functions) are employed to simulate the frequency behavior of power systems under disturbances. These models are particularly effective for representing renewable energy-operated subsystems (REOS), as discussed in the subsequent sections [52], [53].

2.2. Power System Modeling

Fig. 1 depicts a simplified block diagram of the investigated µG system. The system's transient characteristics are formulated using a mathematical framework referenced in [54]-[56]. The core principle involves analyzing how deviations between generated power and load demand (expressed as the difference (ΔPd - ΔPL)) influence changes in system frequency (Δf). This frequency shift serves as an indicator of the system's ability to dynamically adjust to energy supply-demand imbalances.

$$\mathrm{f} = \left(\frac{1}{M}\right).\Delta\mathrm{Pd} - \left(\frac{1}{M}\right).-\Delta\mathrm{PL} - \left(\frac{D}{M}\right).\Delta\mathrm{f} \tag{1}$$

The dynamic behavior of the DsG is formulated as follows:

$$\Delta\mathrm{Pd} = \left(\frac{1}{T\mathrm{d}}\right).\Delta\mathrm{Pg} - \left(\frac{1}{T\mathrm{d}}\right).\Delta\mathrm{Pd} \tag{2}$$

The governing system dynamics are represented by the following expression:

$$\Delta\mathrm{Pg} = \left(\frac{1}{T\mathrm{g}}\right).\Delta\mathrm{Pc} - \left(\frac{1}{R.T\mathrm{d}}\right).\Delta\mathrm{f} - \left(\frac{1}{T\mathrm{g}}\right).\Delta\mathrm{Pg} \tag{3}$$

The µG's dynamic behavior is governed by a complex interaction of system parameters and state variables. Within this model, ΔPg represents changes in the governor signal, ΔPd denotes variations in the DsG's power output, and Δf captures deviations in system frequency. These dynamics are largely driven by fluctuations in load demand (ΔPL) and are counteracted by the supplementary control signal (ΔPc). The system's inertia (M) plays a critical role in buffering frequency disturbances, while the damping coefficient (D) regulates the attenuation of oscillations. Furthermore, the sensitivity of the governor to frequency deviations is expressed through the droop characteristic (R). Temporal aspects of the control system, such as governor and turbine response delays, are encapsulated by the time constants Tg and Td, respectively. To accurately reflect the evolution of these states over time, the model employs differential equations that describe the time rates of change for frequency ($\frac{\mathrm{df}}{\mathrm{dt}}$), diesel generation ($\frac{\mathrm{dPd}}{\mathrm{dt}}$), and governor action ($\frac{\mathrm{dPg}}{\mathrm{dt}}$) [57]-[59].

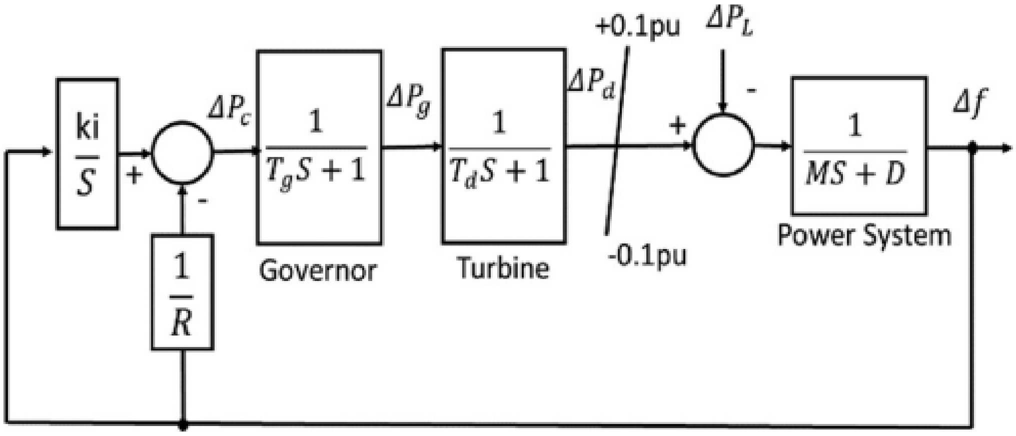

Fig. 1. Structural layout of the µG dynamic model

2.3. Modeling of the DsG and PV System

The DsG system comprises key subsystems, notably the governor and turbine, which play a critical role in dynamic performance and frequency regulation. The FO transfer function models for these components are presented in Equations (4) through (6). The transfer function of the diesel generator, which relates the frequency deviation (Δf) to the change in power output (ΔP_{DsG}) is given by:

$$G_{DsG} = \frac{K_{DsG}}{1 + ST_{DsG}} = \frac{\Delta P_{DsG}}{\Delta f} \tag{4}$$

The turbine dynamics are modeled by a simple first-order lag system:

$$G_{\text{Turbine}}(s) = \frac{1}{ST} \tag{5}$$

Similarly, the governor's response is represented as:

$$G_g(s) = \frac{1}{1 + ST_{gi}} \tag{6}$$

Where K_{DsG} is the gain of the DsG, $T_{DsG}$is its time constant, T is the time constant of the turbine, and T_{gi} is the time constant associated with the governor dynamics.

These models collectively define the frequency control behavior of the DsG subsystem under transient conditions. The frequency behavior and power output of the PV system are described using the mathematical expressions provided in Equations (7) and (8) [60], [61]. The generated power from the PV array is influenced by solar irradiance (∅), ambient temperature (T_a), and surface area (S), and can be expressed as:

$$P_{PV} = \emptyset S\eta\{1 - 0.005(T_a + 25)\} \tag{7}$$

The dynamic response of the PV system is represented by a first-order transfer function (TF), which relates the change in power output (P_{PV}) to variations in irradiance (Φ):

$$G_{PV} = \frac{K_{PV}}{1 + ST_{PV}} = \frac{\Delta P_{PV}}{\emptyset} \tag{8}$$

where S is the surface area of the PV module (m²), K_{PV} is the system gain, and T_{PV} is the time constant of the PV system's dynamic response. This model captures both the steady-state power generation characteristics and the transient frequency behavior of the PV component within the µG.

2.4. EV Modelling

Fig. 2 presents the dynamic representation of an aggregated EV unit. In this model, T_{EV} denotes the time constant associated with the EV system, while U_{EV} refers to the control signal applied to the EV's input, driven by the system's F deviation. The transfer function characterizing the EV's power response is modeled as an FO system, which filters the control input to produce the active power variation ΔP_{EV}. In this study, the model parameters are assigned as $T_{EV} = 0.35$ and the nominal power output P_{EV}^{rated}=2.2. The controller for the EV is designed using a robust H_∞ control approach, ensuring system stability and responsiveness under frequency fluctuations, as detailed in [60], [62]-[64].

FO-TF:

$$G_{EV}(s) = \frac{1}{1+ST_{EV}}(7)$$

Power output of EV unit:

$$P_{EV}(S) = U_{EV}(S).G_{EV}(s)(8)$$

Power deviation from rated value:

$$\Delta P_{EV}(S) = P_{EV}(S) - P_{\text{EV}}^{rated}(9)$$

where T_{EV} is the time constant of the EV unit (sec), $U_{EV}(S)$ is the input control signal influenced by frequency deviation, $P_{EV}(S)$ is the output power of the EV unit, and $\Delta P_{EV}(S)$ is the power deviation from the rated output.

3. Hybrid Adaptive Control using WSA and BE Technique

3.1. WSA Algorithm

The WSA is a hybrid metaheuristic optimization method inspired by the principles of radar wave propagation. It is specifically engineered to strike a balance between broad search space exploration and precise local exploitation, making it particularly effective for adaptive control tasks such as LFC in μGs [65].

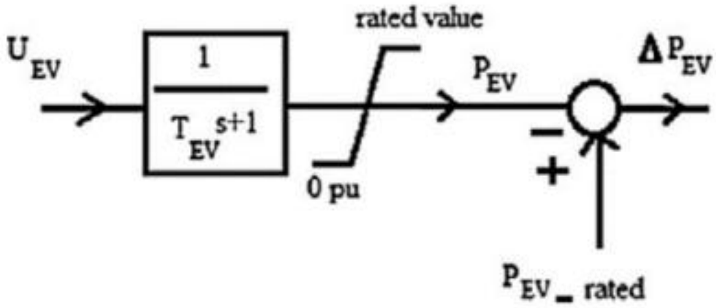

Fig. 2. Frequency-controlled power response model of the EV unit [56]

WSA begins by initializing a population of particles, each defined in a d-dimensional space. The initial positions of the particles are uniformly distributed within the lower (lb) and upper (ub) bounds of the search domain, using the equation:

$$W = lb + x^*(ub - lb) \tag{9}$$

Each particle's position is evaluated using an objective function f , yielding a fitness vector:

$$F = [f([W_{11}, W_{12}, \cdots W_{1d}]); f([W_{21}, W_{22}, \cdots W_{2d}]) \cdots f([W_{n1}, W_{n2}, \cdots W_{nd}])] \tag{10}$$

To foster diversity and prevent premature convergence, WSA performs a global exploration step that modifies particle positions through scaling and translation:

$$W_i^{\text{new}} = W_{\min} + r_1 \cdot (W_{\max} - W_{\min}) \tag{11}$$

This update is accepted only if the new solution outperforms the average fitness:

$$W_i = W_i^{\text{new}} \text{ if } f\left(W_i^{\text{new}}\right) \leq f_{\text{mean}} \tag{12}$$

For local search enhancement, WSA simulates wave emission, allowing particles to adjust around the best-known solution. This is modeled by:

$$W_i^{\text{new}} = W_{\text{best}} + \frac{(W_{li} - W_{\text{beat}}) \cdot (1 + m_i)}{\sigma} \tag{13}$$

$$\begin{cases} W_i = W_i^{\text{new}} \text{ if } f\left(W_i^{\text{new}}\right) \leq f_{\max} \\ W_i = W_i \text{ if } f\left(W_i^{\text{new}}\right) > f_{\max} \end{cases} \tag{14}$$

Here, σ is a dynamically adjusted wave coefficient given by:

$$\sigma = -(5t/T - 2)/\sqrt{25(5t/T - 2)^2} + 0.7 \tag{15}$$

This step is accepted when it yields a better fitness value:

$$\begin{cases} W_i = W_i^{\text{pew}} & \text{if } f\left(W_i^{\text{new}}\right) \leq f(W_i) \\ W_i = W_i & \text{if } f\left(W_i^{\text{new}}\right) > f(W_i) \end{cases} \tag{16}$$

WSA further mimics wave reflection by estimating gradients using central difference approximation:

$$\begin{gathered} g_i = \left(f(W_{+\alpha i}) - f(W_{-\alpha i})\right)/2e \\ W_i = W_i - \alpha \cdot g_i \end{gathered} \tag{17}$$

In the reception phase, the algorithm applies probabilistic corrections inspired by radar echo analysis. Depending on a random threshold r_5, two update mechanisms are used:

$$\begin{cases} W_i^{\text{new}} = W_i + \delta \cdot r_2 \cdot (W_{\text{best}} - W_i) + \eta \cdot \cos\left(\frac{\pi i}{n}\right) \cdot (W_{\text{best}} - W_i) & \text{if } r_5 \leq 0.7 \\ W_i^{\text{new}} = W_i + \lambda \cdot r_3 \cdot (W_{\text{best}} - W_i) + 0.5 \cdot r_4 \cdot (1-\lambda) \cdot (W_{\text{best}}^{*} - W_i) & \text{if } r_5 > 0.7 \end{cases} \tag{18}$$

Each new position is retained only if it improves the fitness:

$$\begin{cases} W_i = W_i^{\text{pew}} & \text{if } f\left(W_i^{\text{new}}\right) \leq f(W_i) \\ W_i = W_i & \text{if } f\left(W_i^{\text{new}}\right) > f(W_i) \end{cases} \tag{19}$$

To address boundary violations, any particle exceeding the defined limits is reassigned a random position within bounds:

$$W_i = lb + r \cdot (ub - lb) \text{ if } W_i > ub \text{ or } W_i < lb \tag{20}$$

Through this structured sequence of exploration, wave-based local search, gradient correction, and boundary handling, WSA ensures an adaptive and robust search mechanism. Its dynamic nature and convergence reliability make it highly effective for LFC optimization in complex, variable environments like modern µGs.

3.2. BEI Method

The BE mechanism, inspired by the way air pressure alters a balloon's size, captures how disturbances and uncertainties in system parameters impact the TF. $G_i(\mathrm{s})$ at each iteration. As shown in Fig. 3, the BE identifier modifies the optimization process by adaptively tuning the OF during every evaluation cycle. This enhances the algorithm's capacity to manage dynamic challenges within µG control. At any given iteration i, the system's online transfer function is estimated as:

$$G_i(\mathrm{s}) = \frac{Y_i(s)}{U_i(s)} \tag{21}$$

Here, $G_i(\mathrm{s})$ represents the current transfer function, computed based on the system's input-output relationship. This transfer function evolves iteratively, depending on its preceding value. $G_{i-1}(s)$, using:

$$\mathrm{G_i(s)} = AL_i G_{i-1}(s) \tag{22}$$

The previous transfer function $G_{i-1}(s)$ itself is defined in terms of a nominal model $G_0(s)$ and a cumulative gain factor ρ_i:

$$G_{i-1}(s) = \rho_i G_0(s) \tag{23}$$

The cumulative gain ρ_i is the product of all gain updates from the initial step to the current iteration:

$$\rho_i = \prod_{n=1}^{i-1} AL_n \tag{24}$$

Substituting back, the full expression for $G_i(s)$ becomes:

$$G_i(s) = AL_i \rho_i G_0(s) \tag{25}$$

3.3. WSA+BE Technique

Fig. 4 presents a simplified µG layout designed to facilitate the parameter identification of a second-order closed-loop transfer function for the regulated system zone. The dynamic model is expressed as:

$$\mathrm{T.F} = \frac{wn^2}{S^2 + 2\eta Wn + Wn^2} = \frac{\frac{Ki}{Mo}}{S^2 + \left(\frac{\left(Do + \frac{1}{Ro}\right)}{Mo}\right)S + \frac{Ki}{Mo}} \tag{26}$$

In this formulation:

Do, Ro , and Mo denote the nominal values for the damping coefficient, droop characteristic, and inertia constant, respectively. The natural frequency Wn and damping ratio η are derived as:

$$\omega_n = \sqrt{\mathrm{Ki/Mo}}\,, \eta = \frac{\frac{(Do+\frac{1}{Ro})}{Mo}}{2\omega_n} \tag{27}$$

From these parameters, key time-domain specifications are calculated:

- Rise time T_r
- Settling time T_s
- Maximum overshoot M_P

$$T_r = \frac{\pi-\sqrt{(1-\eta^2)}}{\omega_n\sqrt{(1-\eta^2)}},\ \ T_s = \frac{4}{\eta\omega_n},\ M_P = e^{\frac{-\pi\,\eta}{\sqrt{(1-\eta^2)}}} \tag{28}$$

These expressions are integrated into the objective function used by the Harris Hawks Optimization (HHO) algorithm, enhanced with the Balloon Effect (BE) mechanism. The cost function to be minimized is:

$$J = min \sum (T_r + T_s + M_P) \tag{29}$$

This objective function is directly influenced by the adaptive gain and tuning coefficient, enabling the system to efficiently respond to uncertainties and dynamic variations within the µG.

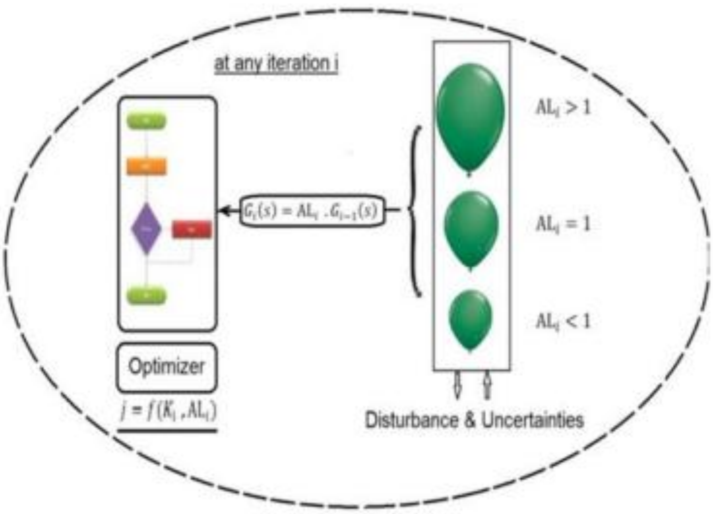

Fig. 3. Illustration of the BE mechanism for iterative gain adjustment under system disturbances [66]

4. Results and Discussions

To assess the effectiveness of the proposed hybrid controller based on WSA+BE, extensive simulation tests were conducted on a multi-energy µG composed of a 20 MW DsG, a PV unit, and an aggregated EV system. The simulations were designed to evaluate the system's frequency response under dynamic load fluctuations and step disturbances, with a particular focus on the adaptive behavior of the controller in the presence of time-varying conditions. The parameters used to model the µG system are outlined in Table 2, which includes the nominal frequency, generator specifications, time constants, inertia, damping, droop characteristics, and control parameters. These values were selected to reflect realistic operating conditions for an isolated microgrid incorporating diesel generation, PV systems, and an aggregated EV unit. The selection ensures that the simulation results are both credible and representative of actual µG dynamics.

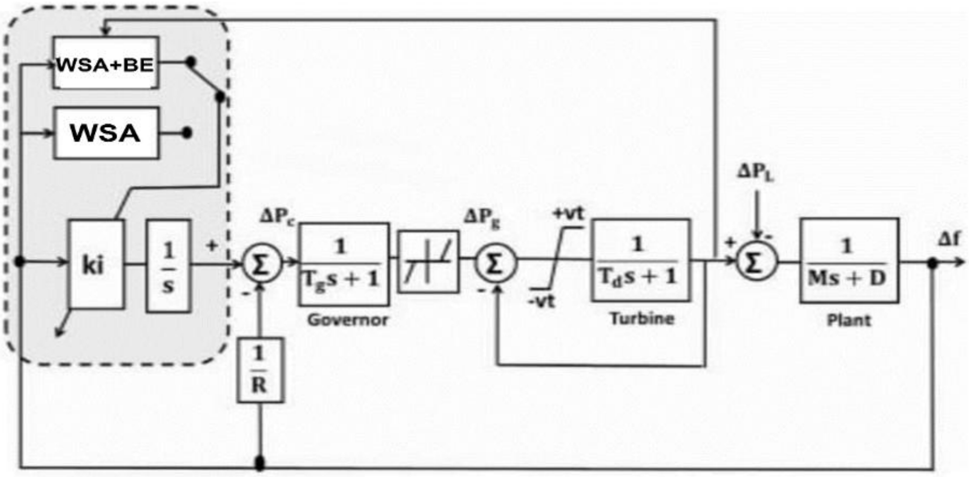

Fig. 4. Control architecture of the µG model with integrated WSA and BE mechanism

To enable a fair comparison of optimization techniques, the configurations of each algorithm used for controller tuning are presented in Table 3. This includes WSA+BE, standalone WSA, Gorilla Troops Optimization (GTO), Sine Cosine Optimization (SCO), and the Jaya algorithm. Each method is parameterized with an equal population size and iteration limit, while varying in control strategies, update mechanisms, and degrees of adaptability. These differences significantly influence the convergence behavior and suitability of each optimizer for real-time LFC in µGs.

Table 2. µG system parameters

Parameter	Symbol	Value	Unit	Description
System nominal frequency	f_0	50	Hz	Base frequency of the µG
Rated power of DsG	ΔP_{DsG}	20	MW	Generator size
Governor time constant	T_g	0.2	sec	Response time of the governor
Turbine time constant	T_t	0.3	sec	Response time of the diesel turbine
Inertia constant	M	10	s	Equivalent system inertia
Damping coefficient	D	0.015	pu/Hz	Frequency sensitivity of load
Droop characteristic	R	2.4	Hz/pu	Frequency-power characteristic of the governor
Nominal load	P_L	15	MW	Average daily load
Load fluctuation range	–	±1.5	MW	Step disturbance magnitude
Controller output gain	K_g	1	–	Initial gain for the control signal
Simulation time	–	100	sec	Total runtime for each test
Sampling time	–	0.01	sec	Time step for simulation resolution
BE initial gain	G_0	1	–	Nominal gain before adaptation
Balloon tuning sensitivity	K_i	0.6	–	Scaling factor for system adaptation
Time constant of the EV unit	T_{EV1}	0.38	sec	Response time of EV
	T_{EV2}	038	sec	

4.1. Scenario 1: Frequency and Power Behavior Under a Step Load Increase

To investigate the responsiveness and resilience of the WSA+BE controller, a sudden step increase of 1.5 MW in system load was applied at 10 seconds in an islanded µG environment. This test emulates a realistic challenge in isolated systems, where abrupt increases in demand can lead to severe imbalances in frequency and active power, especially without external grid support or significant inertia. Fig. 5 illustrates the frequency trajectories resulting from five different control strategies: Jaya, SCO, GTO, WSA, and the proposed WSA+BE. The Jaya algorithm yielded the weakest dynamic performance, experiencing a peak frequency deviation of 0.215 Hz and requiring 21.4 seconds to settle, along with noticeable oscillatory behavior. The SCO method slightly improved upon this, lowering the deviation to 0.187 Hz but still encountering moderate overshoots and damping issues. The GTO controller provided enhanced damping characteristics, restricting deviation to 0.165 Hz and stabilizing the system within 14.8 seconds. WSA demonstrated further refinement, achieving a faster recovery time of 10.6 seconds and minimizing the frequency drop to 0.138 Hz. However, the hybrid WSA+BE controller outperformed all other techniques. It recorded the smallest frequency deviation of just 0.095 Hz and completed system stabilization in only 6.7 seconds, with no perceptible oscillations. This marked improvement stems from the Balloon Effect's real-time adaptability, which dynamically tunes control parameters to improve transient response.

Table 3. Parameters of each algorithm

Parameter	WSA+BE	WSA	GTO	SCO	Jaya
Population size	30	30	30	30	30
Maximum iterations	100	100	100	100	100
Main control parameter	Wave coefficient k	Wave coefficient k	$\beta = 3$, $\alpha = 0.03$	a = 2	–
Position update strategy	Wave propagation + BE modulation	Wave propagation	Hierarchy-based	Sine-cosine update	Best-worst guided
Exploration-exploitation switch	Adaptive to dynamic disturbances	Fitness-based update	By coefficients	Random-based	Implicit
Randomness type	Echo-based + gradient	Wave-based	Random leader-follower	Sinusoidal	Uniform random
Notable feature	Real-time adaptation via BE	Balanced exploration/exploitation	Troop dynamics	Simple sine behavior	Parameter-free design
Suitability for real-time use	High	Moderate	Moderate	Low	Low

To complement the frequency analysis, Fig. 6 depicts the active power response under the same disturbance scenario. The Jaya and SCO controllers induced significant oscillations and sluggish convergence, indicating insufficient damping capacity. GTO offered a partial reduction in oscillation amplitude but remained vulnerable to the load change intensity. In contrast, WSA enabled a smoother and more controlled power profile, validating its more balanced controller gains. Notably, the WSA+BE controller showcased the most efficient power regulation, swiftly mitigating the disturbance and achieving steady-state power restoration with minimal overshoot. Its coordinated control of the diesel generator and electric vehicle units enabled a rapid return to the nominal 15 MW output, outperforming all other approaches in both precision and response time.

Table 4 provides a quantitative performance comparison, listing each controller's frequency deviation, settling time, oscillatory severity, and overall ranking. The results decisively highlight the robustness and adaptability of the WSA+BE approach in managing abrupt load disturbances within microgrid systems.

Table 4. Performance comparison under sudden load disturbance

Technique	Max Frequency Deviation (Hz)	Settling Time (s)	Oscillation Presence	Stability Rating
Jaya	0.215	21.4	High	Poor
SCO	0.187	17.9	Moderate	Fair
GTO	0.165	14.8	Low	Good
WSA	0.138	10.6	Very Low	Very Good
WSA+BE	0.095	6.7	None	Excellent

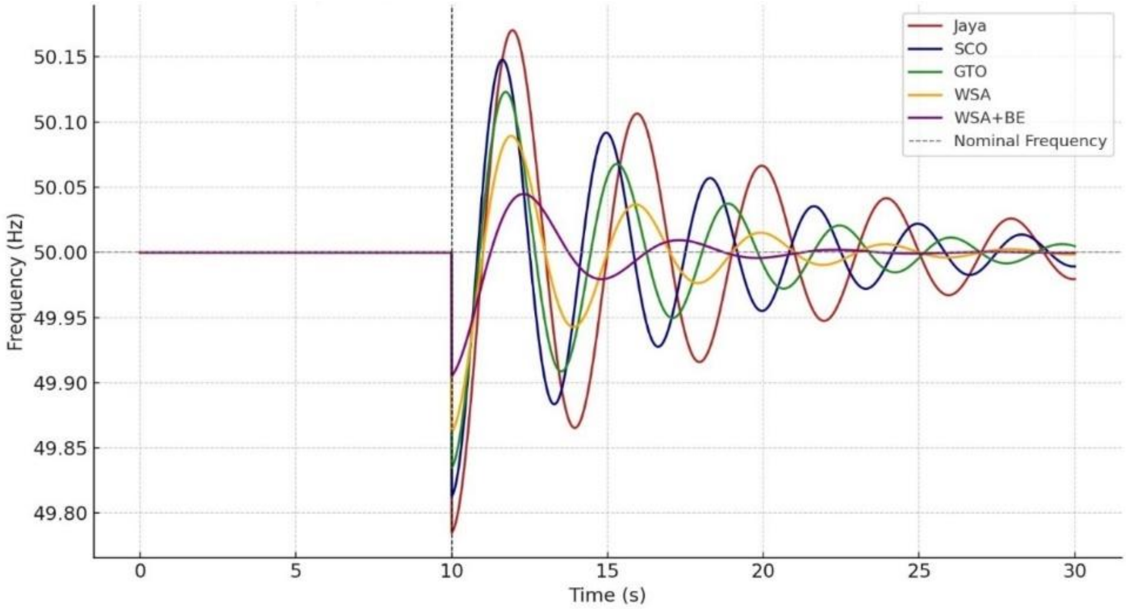

Fig. 5. Frequency response of the μG system under a sudden load increase of 1.5 MW using different optimization-based controllers

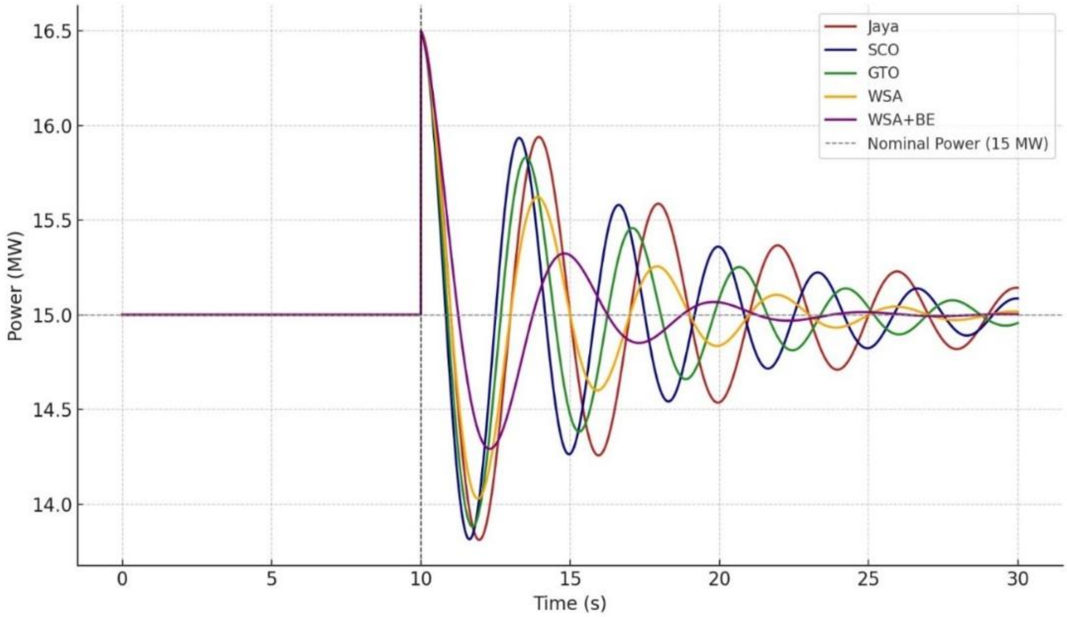

Fig. 6. Active power response corresponding to the load disturbance scenario, highlighting the damping behavior of each technique

4.2. Scenario 2: System Response to Sudden PV Output Reduction

In continuation of the stress test from Scenario 1, this scenario explores the μG's dynamic behavior under a different yet equally critical disturbance: a sharp drop in solar power output, initiated at t = 12 seconds. This simulates the sudden loss of PV generation due to cloud cover or irradiance variability (an increasingly common event in RES-dominated grids). Unlike the demand-side disturbance previously analyzed, this case focuses on the grid's capability to absorb renewable generation deficits, which pose unique challenges due to their non-inertial characteristics. As depicted in Fig. 7, frequency response profiles under this event reveal pronounced differences between controllers. The SCO controller experienced the highest frequency deviation, reaching approximately +0.032 Hz, and took more than 17 seconds to settle, accompanied by noticeable oscillations. Jaya fared slightly better but still recorded a deviation of 0.018 Hz, with limited damping. These findings align with their earlier poor performance under load disturbances.

Conversely, the proposed WSA+BE controller exhibited outstanding resilience, containing the F-deviation to just 0.006 Hz and restoring stability in under 6 seconds. This highlights the controller's ability to adjust in real time to generation-side perturbations, maintaining system frequency close to nominal despite a loss of supply. It is worth noting the contrasting system dynamics between the two scenarios. While load disturbances tend to produce symmetrical deviations owing to the inertial reaction of synchronous machines, the PV drop resulted in an asymmetric frequency response. This is primarily due to the lack of rotating mass in PV systems, which shifts the burden of compensation to inertia-equipped elements such as diesel generators and EV storage. Fig. 8 shows the corresponding active power adjustments following the PV power reduction of 2.0 MW. Controllers based on Jaya and SCO responded with high overshoots—reaching 0.4 MW and 0.3 MW, respectively—and took considerable time to stabilize. GTO offered improved damping but still could not prevent a delayed transition. In contrast, WSA+BE again demonstrated optimal performance, achieving power stabilization in just 5 s with no observable overshoot or oscillation. This swift and stable compensation is vital for maintaining reliability in PV-integrated μGs.

The comparative assessment of Scenarios 1 and 2 underscores the dual adaptability of WSA+BE to both load increases and renewable generation losses. Its consistently superior performance across different dynamic events confirms its robustness and flexibility (traits essential for modern μG frequency and power management). These findings emphasize the necessity for hybrid, self-adjusting optimization strategies over fixed-parameter approaches, especially in systems subject to high-RES penetration and variable operating conditions.

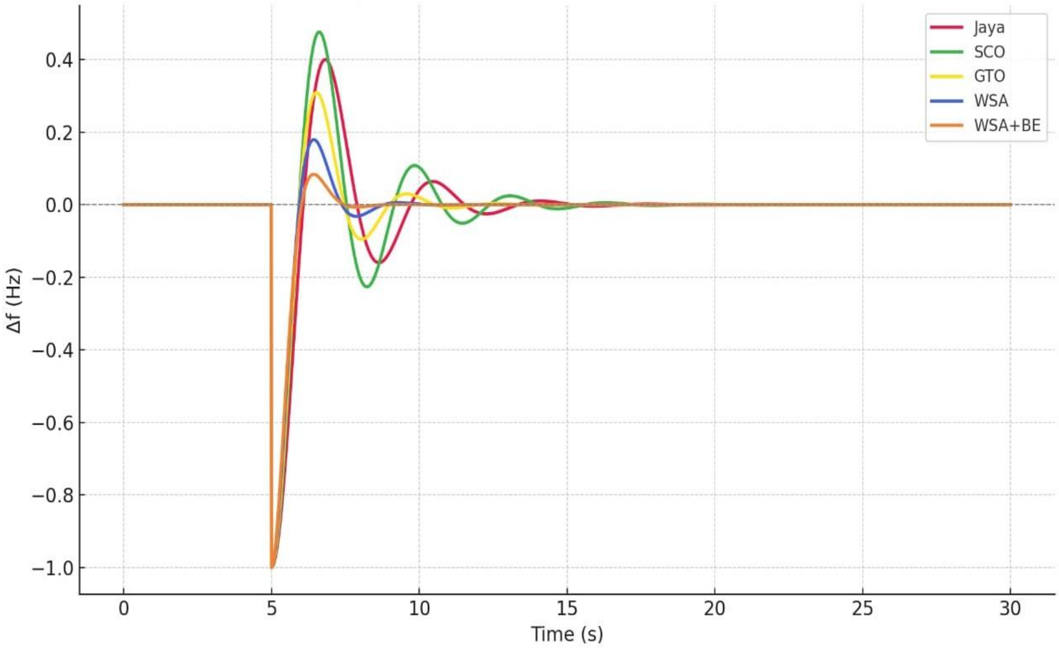

Fig. 7. Frequency trajectories following a sudden drop in PV output, demonstrating each controller's capability in compensating renewable generation losses

4.3. Scenario 3: Adaptability Under Load Fluctuations with EV Bi-Directional Support

Extending the analysis from the previous scenarios, which focused on isolated disturbances, Scenario 3 introduces a more intricate and representative challenge: a continuously varying load profile augmented by active bi-directional EV engagement. This setup mimics the dynamic behavior observed in modern microgrids enriched with prosumers and EV infrastructure, where variability is not abrupt but persistently evolving. Fig. 9 illustrates a load oscillating around a nominal value of 15 MW, modulated by low to medium frequency disturbances that reflect stochastic consumer usage patterns. Such a setting imposes sustained stress on both the frequency regulation and power balancing mechanisms, making it a rigorous test of controller resilience and agility.

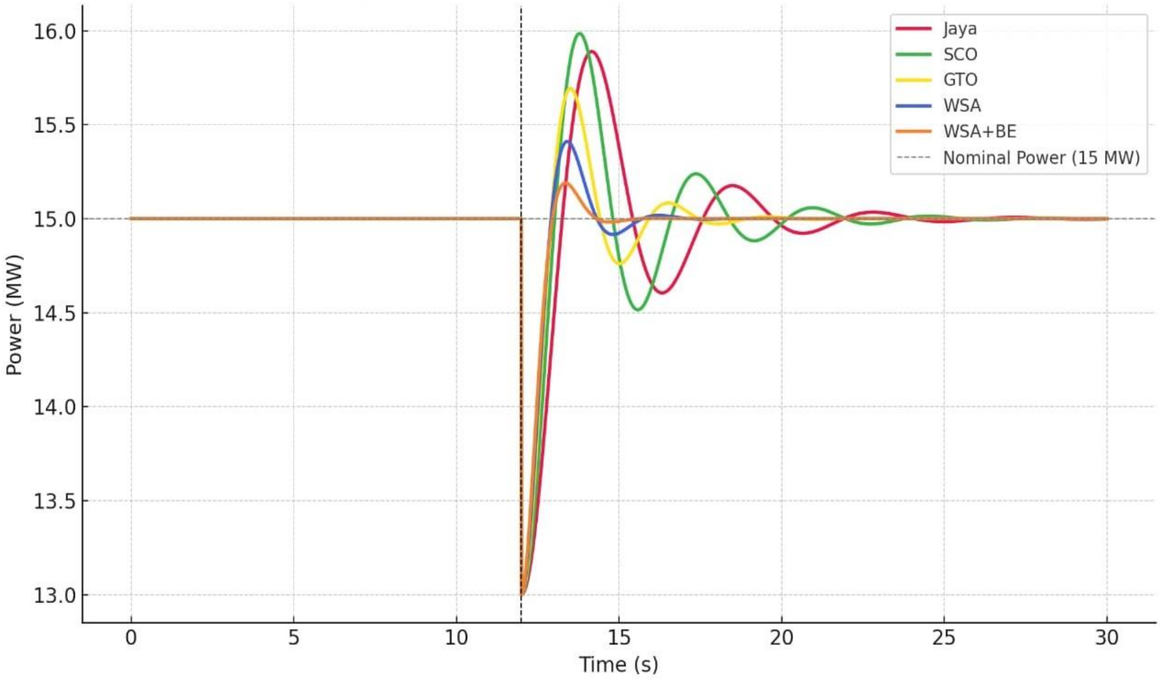

Fig. 8. Power response curves under PV generation loss, emphasizing the effectiveness of the proposed WSA+BE controller in fast compensation

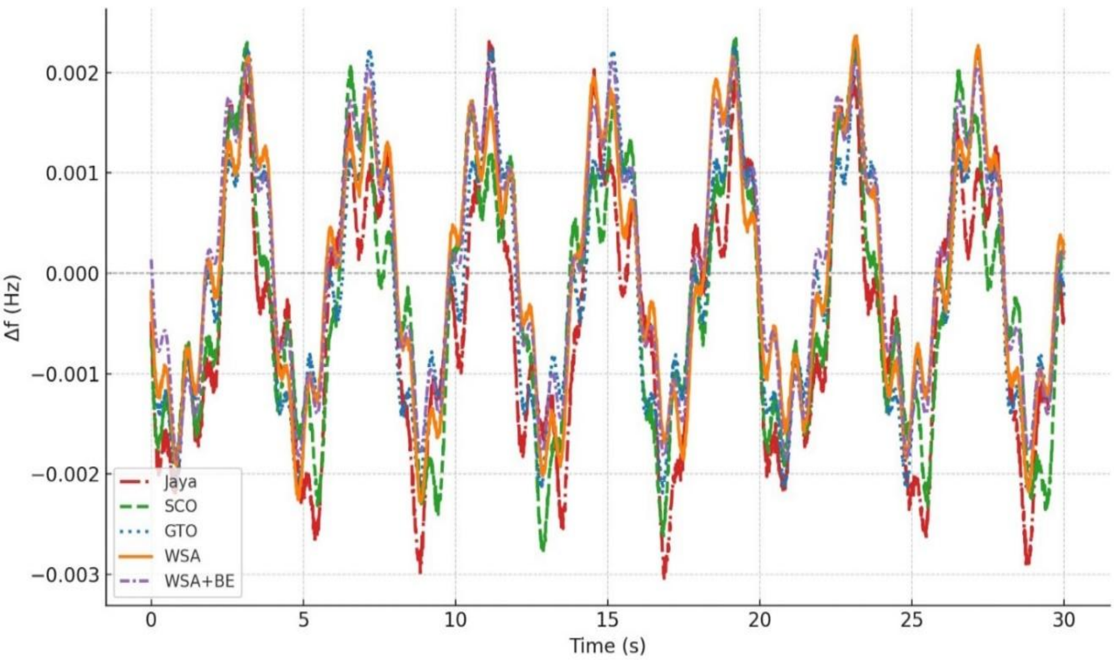

Fig. 9. Load variation profile used in Scenario 3, incorporating low- and mid-frequency fluctuations to simulate prosumer activity

The performance of each controller under this dynamic regime uncovers notable distinctions. Jaya and SCO (as shown in Table 5) exhibit delayed responses with evident overshoots, struggling to synchronize with the shifting load demands. GTO manages a better alignment, yet remains vulnerable to higher-frequency fluctuations. The proposed WSA+BE controller, however, displays superior adaptability, tracking the load smoothly with minimal error. Its response trajectory shows suppressed ripples and seamless slope transitions, emphasizing its capacity for both reactive and proactive control, reinforcing the strengths identified in Scenarios 1 and 2. Complementary power deviation patterns, shown in Fig. 10, reinforce these observations. Whereas traditional controllers allow oscillations beyond ±0.3 MW, WSA+BE confines deviations within ±0.08 MW, reflecting a tightly regulated power flow. This is largely attributed to its efficient coordination with the bi-directional EV, which functions dynamically as both a load and a support source, absorbing or injecting power to cushion variations. Collectively, this scenario underscores the controller's efficacy in handling real-world microgrid conditions characterized by continuous load variation. It demonstrates that WSA+BE is not only effective in mitigating transient disturbances and renewable unpredictability but is also highly adept at managing sustained variability, making it an optimal solution for next-generation distributed energy systems.

Table 5. Performance comparison under fluctuating load (scenario 3)

Technique	Load Tracking Accuracy	Power Deviation Range	Response Smoothness	Overall Stability
Jaya	Low	±0.38 MW	Oscillatory	Poor
SCO	Moderate	±0.34 MW	Fluctuating	Fair
GTO	Good	±0.24 MW	Improved	Good
WSA	Very Good	±0.15 MW	Smooth	Very Good
WSA+BE	Excellent	±0.08 MW	Very Smooth	Excellent

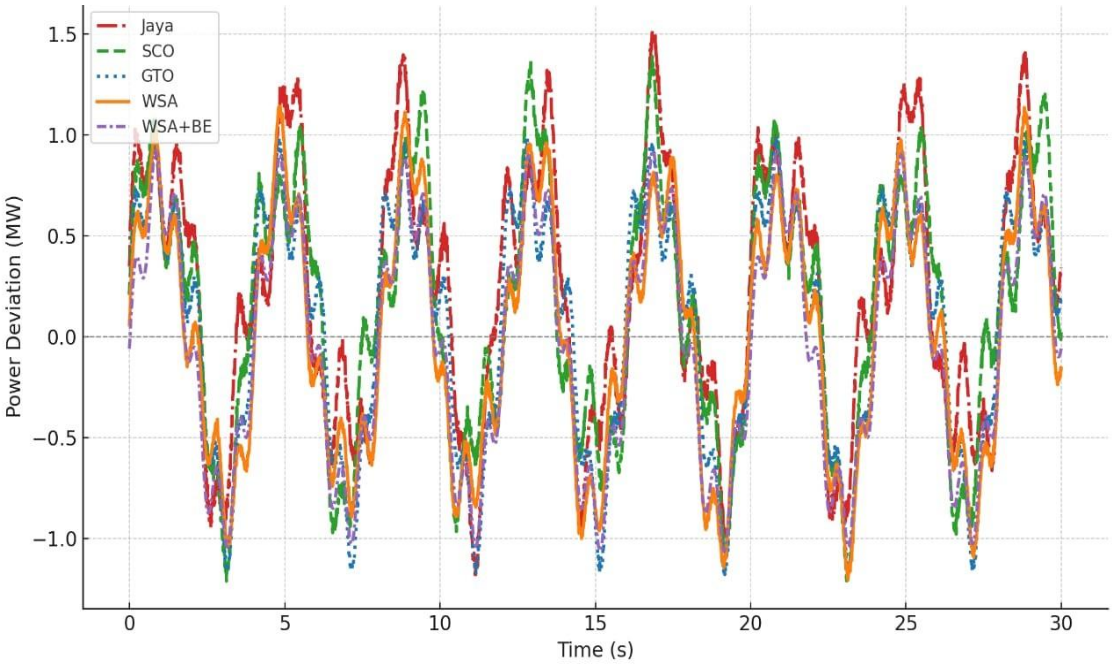

Fig. 10. Power deviation profiles of the μG system under fluctuating load conditions with bi-directional EV participation

5. Conclusions

This work introduced a novel hybrid control strategy that merges the WSA with the BE to enhance load frequency regulation in renewable energy-based microgrids. By uniting WSA's efficient exploration-exploitation balance with BE's adaptive structural tuning, the proposed WSA+BE controller effectively manages the dynamic frequency challenges posed by the variability of solar and wind generation. Through rigorous simulation studies covering three critical disturbance scenarios (sudden load surges, abrupt photovoltaic output loss, and continuous load fluctuation with active EV involvement), the WSA+BE method consistently outperformed both traditional and advanced optimization-based controllers. It delivered the smallest frequency deviations, rapid system stabilization, and highly responsive control trajectories, emphasizing its real-time adaptability to evolving system dynamics. The findings underscore the drawbacks of static tuning and conventional optimization methods in the face of high-RES penetration and variable demand. The inclusion of EVs as dynamic energy assets further intensifies control demands (demands that the WSA+BE framework addresses with remarkable accuracy and robustness. Ultimately, the proposed approach represents a forward-looking advancement in intelligent LFC. It establishes a strong foundation for future exploration into structure-aware, real-time optimization and supports practical extensions toward multi-objective control and hardware-in-the-loop applications, advancing the development of resilient, smart μG infrastructures.

Author Contribution: All authors contributed equally to the main contributor to this paper. All authors read and approved the final paper.

Sustainable Development Goals: Sustainable Development Goals mapped to this document, Affordable and Clean Energy Goal 7.

Data Availability: The data used to support the findings of this study are available at reasonable request from the corresponding author.

Conflicts of Interest: The authors declare that they have no conflicts of interest.

Acknowledgment: The authors extend their appreciation to Prince Sattam bin Abdulaziz University for funding this research work through the project number (PSAU/2025/01/33173).

Funding: The authors extend their appreciation to Prince Sattam bin Abdulaziz University for funding this research work through the project number (PSAU/2025/01/33173).

References

[1] S. Basu *et al.*, "Applications of Snow Ablation Optimizer for Sustainable Dynamic Dispatch of Power and Natural Gas Assimilating Multiple Clean Energy Sources," *Engineering Reports*, vol. 7, no. 6, pp. 1-12, 2025, https://doi.org/10.1002/eng2.70211.

[2] M. Awad *et al.*, "A review of water electrolysis for green hydrogen generation considering PV/wind/hybrid/hydropower/geothermal/tidal and wave/biogas energy systems, economic analysis, and its application," *Alexandria Engineering Journal*, vol. 87, pp. 213-239, 2024, https://doi.org/10.1016/j.aej.2023.12.032.

[3] M. M. Mahmoud, "Improved current control loops in wind side converter with the support of wild horse optimizer for enhancing the dynamic performance of PMSG-based wind generation system," *International Journal of Modelling and Simulation*, vol. 43, no. 6, pp. 952-966, 2023, https://doi.org/10.1080/02286203.2022.2139128.

[4] S. Heroual *et al.*, "Enhancement of Transient Stability and Power Quality in Grid- Connected PV Systems Using SMES," *International Journal of Robotics and Control Systems*, vol. 5, no. 2, pp. 990-1005, 2025, https://doi.org/10.31763/ijrcs.v5i2.1760.

[5] M. S. Priyadarshini, S. A. E. M. Ardjoun, A. Hysa, M. M. Mahmoud, U. Sur, and N. Anwer, "Time-domain Simulation and Stability Analysis of a Photovoltaic Cell Using the Fourth-order Runge-Kutta Method and Lyapunov Stability Analysis," *Buletin Ilmiah Sarjana Teknik Elektro*, vol. 7, no. 2, pp. 214-230, 2025, https://doi.org/10.12928/biste.v7i2.13233.

[6] Y. Maamar *et al.*, "A Comparative Analysis of Recent MPPT Algorithms (P&O\INC\FLC) for PV Systems," *Journal of Robotics and Control (JRC)*, vol. 6, no. 4, pp. 1581-1588, 2025, https://doi.org/10.18196/jrc.v6i4.25814.

[7] I. M. Elzein, Y. Maamar, M. M. Mahmoud, M. I. Mosaad, and S. A. Shaaban, "The Utilization of a TSR-MPPT-Based Backstepping Controller and Speed Estimator Across Varying Intensities of Wind Speed Turbulence," *International Journal of Robotics and Control Systems*, vol. 5, no. 2, pp. 1315-1330, 2025, https://doi.org/10.31763/ijrcs.v5i2.1793.

[8] T. Boutabba *et al.*, "Design of a Small Wind Turbine Emulator for Testing Power Converters Using dSPACE 1104," *International Journal of Robotics and Control Systems*, vol. 5, no. 2, pp. 698-712, 2025, https://doi.org/10.31763/ijrcs.v5i2.1685.

[9] O. Makram Kamel, I. M. Elzein, M. M. Mahmoud, A. Y. Abdelaziz, M. M. Hussein, and A. A. Zaki Diab, "Effective energy management strategy with a novel design of fuzzy logic and JAYA-based controllers in isolated DC/AC microgrids: A comparative analysis," *Wind Engineering*, vol. 49, no. 1, pp. 199-222, 2025, https://doi.org/10.1177/0309524X241263518.

[10] A. M *et al*., "Prediction of Optimum Operating Parameters to Enhance the Performance of PEMFC Using Machine Learning Algorithms," *Energy Exploration & Exploitation*, vol. 43, no. 2, pp. 676-698, 2024, https://doi.org/10.1177/01445987241290535.

[11] M. Islam, F. Yang, and M. Amin, "Control and optimisation of networked microgrids: A review," *IET Renewable Power Generation*, vol. 15, no. 6, pp. 1133-1148, 2021, https://doi.org/10.1049/rpg2.12111.

[12] R. G. Allwyn, A. Al-Hinai, and V. Margaret, "A comprehensive review on energy management strategy of microgrids," *Energy Reports*, vol. 9. pp. 5565-5591, 2023, https://doi.org/10.1016/j.egyr.2023.04.360.

[13] M. Hamidieh and M. Ghassemi, "Microgrids and Resilience: A Review," *IEEE Access*, vol. 10, pp. 106059-106080, 2022, https://doi.org/10.1109/ACCESS.2022.3211511.

[14] J. Heidary, M. Gheisarnejad, H. Rastegar, and M. H. Khooban, "Survey on microgrids frequency regulation: Modeling and control systems," *Electric Power Systems Research*, vol. 213, p. 108719, 2022, https://doi.org/10.1016/j.epsr.2022.108719.

[15] K. S. Mohammad and C. R. Kumar, "Optimal control strategy of photovoltaic system based autonomous micro grid for power quality improvement," *Indonesian Journal of Electrical Engineering and Computer Science (IJEECS)*, vol. 32, no. 2, pp. 598-611, 2023, http://doi.org/10.11591/ijeecs.v32.i2.pp598-611.

[16] R. Moumni, K. Laroussi, I. Benlaloui, M. M. Mahmoud, and M. F. Elnaggar, "Optimizing Single-Inverter Electric Differential System for Electric Vehicle Propulsion Applications," *International Journal of Robotics and Control Systems*, vol. 4, no. 4, pp. 1772-1793, 2024, https://doi.org/10.31763/ijrcs.v4i4.1542.

[17] B. Modu, M. P. Abdullah, M. A. Sanusi, and M. F. Hamza, "DC-based microgrid: Topologies, control schemes, and implementations," *Alexandria Engineering Journal*, vol. 70. pp. 61-92, 2023, https://doi.org/10.1016/j.aej.2023.02.021.

[18] N. Altin, S. E. Eyimaya, and A. Nasiri, "Multi-Agent-Based Controller for Microgrids: An Overview and Case Study," *Energies*, vol. 16, no. 5, p. 2445, 2023, https://doi.org/10.3390/en16052445.

[19] A. M. Aboelezz, B. E. Sedhom, M. M. El-Saadawi, A. A. Eladl, and P. Siano, "State-of-the-Art Review on Shipboard Microgrids: Architecture, Control, Management, Protection, and Future Perspectives," *Smart Cities*, vol. 6, no. 3. pp. 1435-1484, 2023, https://doi.org/10.3390/smartcities6030069.

[20] S. Ahmad, M. Shafiullah, C. B. Ahmed and M. Alowaifeer, "A Review of Microgrid Energy Management and Control Strategies," *IEEE Access*, vol. 11, pp. 21729-21757, 2023, https://doi.org/10.1109/ACCESS.2023.3248511.

[21] A. F. A. Ahmed, I. M. Elzein, M. M. Mahmoud, S. A. E. M. Ardjoun, A. M. Ewias, and U. Khaled, "Optimal Controller Design of Crowbar System for DFIG-based WT: Applications of Gravitational Search Algorithm," *Buletin Ilmiah Sarjana Teknik Elektro*, vol. 7, no. 2, pp. 122-137, 2025, https://doi.org/10.12928/biste.v7i2.13027.

[22] F. Menzri, T. Boutabba, I. Benlaloui, H. Bawayan, M. I. Mosaad, and M. M. Mahmoud, "Applications of hybrid SMC and FLC for augmentation of MPPT method in a wind-PV-battery configuration," *Wind Engineering*, vol. 48, no. 6, pp. 1186-1202, 2024, https://doi.org/10.1177/0309524X241254364.

[23] H. Grover, A. Verma, and T. S. Bhatti, "DOBC-based frequency & voltage regulation strategy for PV-diesel hybrid microgrid during islanding conditions," *Renewable Energy*, vol. 196, pp. 883-900, 2022, https://doi.org/10.1016/j.renene.2022.06.140.

[24] X. Gong and X. Wang, "A novel Koopman-inspired method for the secondary control of microgrids with grid-forming and grid-following sources," *Applied Energy*, vol. 333, p. 120631, 2023, https://doi.org/10.1016/j.apenergy.2022.120631.

[25] Z. Chu, G. Cui and F. Teng, "Scheduling of Software-Defined Microgrids for Optimal Frequency Regulation," *IEEE Transactions on Sustainable Energy*, vol. 15, no. 3, pp. 1715-1728, 2024, https://doi.org/10.1109/TSTE.2024.3368656.

[26] C. Zhong, H. Li, Y. Zhou, Y. Lv, J. Chen, and Y. Li, "Virtual synchronous generator of PV generation without energy storage for frequency support in autonomous microgrid," *International Journal of Electrical Power & Energy Systems*, vol. 134, p. 107343, 2022, https://doi.org/10.1016/j.ijepes.2021.107343.

[27] M. A. El-Hameed, M. M. Elkholy, and A. A. El-Fergany, "Efficient frequency regulation in highly penetrated power systems by renewable energy sources using stochastic fractal optimiser," *IET Renewable Power Generation*, vol. 13, no. 12, pp. 2174-2183, 2019, https://doi.org/10.1049%2Fiet-rpg.2019.0186.

[28] J. Liu, Y. Miura and T. Ise, "Comparison of Dynamic Characteristics Between Virtual Synchronous Generator and Droop Control in Inverter-Based Distributed Generators," *IEEE Transactions on Power Electronics*, vol. 31, no. 5, pp. 3600-3611, 2016, https://doi.org/10.1109/TPEL.2015.2465852.

[29] A. M. Ewais, A. M. Elnoby, T. H. Mohamed, M. M. Mahmoud, Y. Qudaih, and A. M. Hassan, "Adaptive frequency control in smart microgrid using controlled loads supported by real-time implementation," *PLoS One*, vol. 18, no. 4, p. e0283561, 2023, https://doi.org/10.1371/journal.pone.0283561.

[30] Y. Li, Z. Xu and K. P. Wong, "Advanced Control Strategies of PMSG-Based Wind Turbines for System Inertia Support," *IEEE Transactions on Power Systems*, vol. 32, no. 4, pp. 3027-3037, 2017, https://doi.org/10.1109/TPWRS.2016.2616171.

[31] M. H. Fini and M. E. Hamedani Golshan, "Determining optimal virtual inertia and frequency control parameters to preserve the frequency stability in islanded microgrids with high penetration of renewables," *Electric Power Systems Research*, vol. 154, pp. 13-22, 2018, https://doi.org/10.1016/j.epsr.2017.08.007.

[32] K. Strunz, K. Almunem, C. Wulkow, M. Kuschke, M. Valescudero and X. Guillaud, "Enabling 100% Renewable Power Systems Through Power Electronic Grid-Forming Converter and Control: System Integration for Security, Stability, and Application to Europe," *Proceedings of the IEEE*, vol. 111, no. 7, pp. 891-915, 2023, https://doi.org/10.1109/JPROC.2022.3193374.

[33] H. Ye, W. Pei and Z. Qi, "Analytical Modeling of Inertial and Droop Responses From a Wind Farm for Short-Term Frequency Regulation in Power Systems," *IEEE Transactions on Power Systems*, vol. 31, no. 5, pp. 3414-3423, 2016, https://doi.org/10.1109/TPWRS.2015.2490342.

[34] M. Moafi, M. Marzband, M. Savaghebi, and J. M. Guerrero, "Energy management system based on fuzzy fractional order PID controller for transient stability improvement in microgrids with energy storage," *International Transactions on Electrical Energy Systems*, vol. 26, no. 10, pp. 2087-2106, 2016, https://doi.org/10.1002/etep.2186.

[35] T. Kerdphol, M. Watanabe, K. Hongesombut and Y. Mitani, "Self-Adaptive Virtual Inertia Control-Based Fuzzy Logic to Improve Frequency Stability of Microgrid With High Renewable Penetration," *IEEE Access*, vol. 7, pp. 76071-76083, 2019, https://doi.org/10.1109/ACCESS.2019.2920886.

[36] J. Wang, H. Ouyang, C. Zhang, S. Li, and J. Xiang, "A novel intelligent global harmony search algorithm based on improved search stability strategy," *Scientific Reports*, vol. 13, no. 1, 2023, https://doi.org/10.1038/s41598-023-34736-1.

[37] H. Su, Z. Dong, Y. Liu, Y. Mu, S. Li, and L. Xia, "Symmetric projection optimizer: concise and efficient solving engineering problems using the fundamental wave of the Fourier series," *Scientific Reports*, vol. 14, no. 1, 2024, https://doi.org/10.1038/s41598-024-56521-4.

[38] A. Alkuhayli, U. Khaled, and M. M. Mahmoud, "A Novel Hybrid Harris Hawk Optimization-Sine Cosine Transmission Network," *Energies*, vol. 17, no. 19, p. 4985, 2024, https://doi.org/10.3390/en17194985.

[39] K. E. Fahim, L. C. D. Silva, F. Hussain, and H. Yassin, "A State-of-the-Art Review on Optimization Methods and Techniques for Economic Load Dispatch with Photovoltaic Systems: Progress, Challenges, and Recommendations," *Sustainability*, vol. 15, no. 15, p. 11837, 2023, https://doi.org/10.3390/su151511837.

[40] M. I. A. E. Ali, A. A. Z. Diab and A. A. Hassan, "Adaptive Load Frequency Control Based on Dynamic Jaya Optimization Algorithm of Power System with Renewable Energy Integration," *2019 21st International Middle East Power Systems Conference (MEPCON)*, pp. 202-206, 2019, https://doi.org/10.1109/MEPCON47431.2019.9007955.

[41] W. Long, J. Jiao, X. Liang, S. Cai and M. Xu, "A Random Opposition-Based Learning Grey Wolf Optimizer," *IEEE Access*, vol. 7, pp. 113810-113825, 2019, https://doi.org/10.1109/ACCESS.2019.2934994.

[42] J. Gwak, H. Garg, N. Jan, and B. Akram, "A new approach to investigate the effects of artificial neural networks based on bipolar complex spherical fuzzy information," *Complex & Intelligent Systems*, vol. 9, no. 4, pp. 4591-4614, 2023, https://doi.org/10.1007/s40747-022-00959-4.

[43] S. R. K. Joga *et al.*, "Applications of tunable-Q factor wavelet transform and AdaBoost classier for identification of high impedance faults: Towards the reliability of electrical distribution systems," *Energy Exploration & Exploitation*, vol. 42, no. 6, pp. 2017-2055, 2024, https://doi.org/10.1177/01445987241260949.

[44] M. N. A. Hamid *et al.*, "Adaptive Frequency Control of an Isolated Microgrids Implementing Different Recent Optimization Techniques," *International Journal of Robotics and Control Systems*, vol. 4, no. 3, pp. 1000-1012, 2024, https://doi.org/10.31763/ijrcs.v4i3.1432.

[45] Y. M. Prianka, A. Sharma, C. Biswas, "Integration of Renewable Energy, Microgrids, and EV Charging Infrastructure: Challenges and Solutions," *Control Systems and Optimization Letters*, vol. 2, no. 3, pp. 317-326, 2024, https://doi.org/10.59247/csol.v2i3.142.

[46] S. A. Mohamed, N. Anwer, and M. M. Mahmoud, "Solving optimal power flow problem for IEEE-30 bus system using a developed particle swarm optimization method: towards fuel cost minimization," *International Journal of Modelling and Simulation*, vol. 45, no. 1, pp. 307-320, 2023, https://doi.org/10.1080/02286203.2023.2201043.

[47] S. Heroual, B. Belabbas, Y. Diab, M. M. Mahmoud, T. Allaoui, and N. Benabdallah, "Optimizing Power Flow in Photovoltaic-Hybrid Energy Storage Systems: A PSO and DPSO Approach for PI Controller Tuning," *International Transactions on Electrical Energy Systems*, vol. 2025, no. 1, pp. 1-23, 2025, https://doi.org/10.1155/etep/9958218.

[48] A. Fatah *et al.*, "Design, and dynamic evaluation of a novel photovoltaic pumping system emulation with DS1104 hardware setup: Towards innovative in green energy systems," *PLoS One*, vol. 19, no. 10, p. e0308212, 2024, https://doi.org/10.1371/journal.pone.0308212.

[49] F. Menzri *et al.*, "Applications of Novel Combined Controllers for Optimizing Grid-Connected Hybrid Renewable Energy Systems," *Sustainability*, vol. 16, no. 16, p. 6825, 2024, https://doi.org/10.3390/su16166825.

[50] P. Sinha *et al.*, "Efficient automated detection of power quality disturbances using nonsubsampled contourlet transform & PCA-SVM," *Energy Exploration & Exploitation*, vol. 43, no. 3, pp. 1149-1179, 2025, https://doi.org/10.1177/01445987241312755.

[51] C. Biswas, A. Sharma, and Y. M. Prianka, "Enhancing Energy Flexibility: A Case Study on Peer-to-Peer (P2P) Energy Trading Between Electric Vehicles and Microgrid," *Control Systems and Optimization Letters*, vol. 3, no. 1, pp. 28-35, 2025, https://doi.org/10.59247/csol.v3i1.144.

[52] A. Raj *et al.*, "Wavelet Analysis- Singular Value Decomposition Based Method for Precise Fault Localization in Power Distribution Networks Using k-NN Classifier," *International Journal of Robotics and Control Systems*, vol. 5, no. 1, pp. 530-554, 2025, https://doi.org/10.31763/ijrcs.v5i1.1543.

[53] B. K. Ponukumati *et al.*, "Evolving fault diagnosis scheme for unbalanced distribution network using fast normalized cross-correlation technique," *PLoS One*, vol. 19, no. 10, p. e0305407, 2024, https://doi.org/10.1371/journal.pone.0305407.

[54] J. Morren, S. W. H. de Haan, W. L. Kling and J. A. Ferreira, "Wind turbines emulating inertia and supporting primary frequency control," *IEEE Transactions on Power Systems*, vol. 21, no. 1, pp. 433-434, 2006, https://doi.org/10.1109/TPWRS.2005.861956.

[55] A. T. Hassan *et al*., "Adaptive Load Frequency Control in Microgrids Considering PV Sources and EVs Impacts: Applications of Hybrid Sine Cosine Optimizer and Balloon Effect Identifier Algorithms," *International Journal of Robotics and Control Systems*, vol. 4, no. 2, pp. 941-957, 2024, https://doi.org/10.31763/ijrcs.v4i2.1448.

[56] M. M. Hussein, T. H. Mohamed, M. M. Mahmoud, M. Aljohania, M. I. Mosaad, and A. M. Hassan, "Regulation of multi-area power system load frequency in presence of V2G scheme," *PLoS One*, vol. 18, no. 9, p. e0291463, 2023, https://doi.org/10.1371/journal.pone.0291463.

[57] T. Aziz, Z. Al Dodaev, M. A. Halim, and M. Y. A. Khan, "A Review on Integration Challenges for Hybrid Energy Generation Using Algorithms," *Control Systems and Optimization Letters*, vol. 2, no. 2, pp. 162-171, 2024, https://doi.org/10.59247/csol.v2i2.85.

[58] M. N. Hussain, K. A. Kader, M. S. Ali, A. Ullah, and Z. Al Dodaev, "An Extensive Analysis of the Significance and Difficulties of Microgrids Based on Renewable Energy in Wireless Sensor Networks," *Control Systems and Optimization Letters*, vol. 2, no. 2, pp. 178-183, 2024, https://doi.org/10.59247/csol.v2i2.102.

[59] M. M. Islam, M. T. Akter, H. M. Tahrim, N. S. Elme, and M. Y. A. Khan, "A Review on Employing Weather Forecasts for Microgrids to Predict Solar Energy Generation with IoT and Artificial Neural Networks," *Control Systems and Optimization Letters*, vol. 2, no. 2, pp. 184-190, 2024, https://doi.org/10.59247/csol.v2i2.108.

[60] S. Vachirasricirikul and I. Ngamroo, "Robust controller design of heat pump and plug-in hybrid electric vehicle for frequency control in a smart microgrid based on specified-structure mixed H2/H∞ control technique," *Applied Energy*, vol. 88, no. 11, pp. 3860-3868, 2011, https://doi.org/10.1016/j.apenergy.2011.04.055.

[61] O. M. Lamine *et al*., "A Combination of INC and Fuzzy Logic-Based Variable Step Size for Enhancing MPPT of PV Systems," *International Journal of Robotics and Control Systems*, vol. 4, no. 2, pp. 877-892, 2024, https://doi.org/10.31763/ijrcs.v4i2.1428.

[62] A. Hysa, M. M. Mahmoud, and A. Ewais, "An Investigation of the Output Characteristics of Photovoltaic Cells Using Iterative Techniques and MATLAB ® 2024a Software," *Control Systems and Optimization Letters*, vol. 3, no. 1, pp. 46-52, 2025, https://doi.org/10.59247/csol.v3i1.174.

[63] B. Benbouya *et al*., "Dynamic Assessment and Control of a Dual Star Induction Machine State Dedicated to an Electric Vehicle Under Short- Circuit Defect," *International Journal of Robotics and Control Systems*, vol. 4, no. 4, pp. 1731-1745, 2024, https://doi.org/10.31763/ijrcs.v4i4.1557.

[64] N. Benalia *et al*., "Enhancing electric vehicle charging performance through series-series topology resonance-coupled wireless power transfer," *PLoS One*, vol. 19, no. 8, p. e0309545, 2024, https://doi.org/10.1371/journal.pone.0300550.

[65] A. Kooshari, M. Fartash, P. Mihannezhad, M. Chahardoli, J. AkbariTorkestani, and S. Nazari, "An optimization method in wireless sensor network routing and IoT with water strider algorithm and ant colony optimization algorithm," *Evolutionary Intelligence*, vol. 17, no. 3, pp. 1527-1545, 2024, https://doi.org/10.1007/s12065-023-00847-x.

[66] M. Mahmoudi, H. Jafari and R. Jafari, "Frequency control of Micro-Grid using state feedback with integral control," *2015 20th Conference on Electrical Power Distribution Networks Conference (EPDC)*, pp. 1-6, 2015, https://doi.org/10.1109/EPDC.2015.7330464.